Dissociative recombination of electrons with diatomic molecular cations above dissociation threshold: Application to H_2^+ and HD^+

K. Chakrabarti,[1,2] D. R. Backodissa-Kiminou,[1] N. Pop,[3] J. Zs. Mezei,[1,4,5] O. Motapon,[6] F. Lique,[1] O. Dulieu,[4] A. Wolf,[7] and I. F. Schneider[1]

[1]*LOMC CNRS-UMR-6294, Université du Havre, Le Havre 76058, France*

[2]*Department of Mathematics, Scottish Church College, 1 & 3 Urquhart Square, Kolkata 700 006, India*

[3]*Department of Physical Foundations of Engineering, "Politehnica" University of Timisoara, V. Parvan Street, No.2, Timisoara 300006, Romania*

[4]*Laboratoire Aimé Cotton CNRS-UPR-3321, Université Paris-Sud, Orsay F-91405, France*

[5]*Institute of Nuclear Research of the Hungarian Academy of Sciences, P.O. Box 51, Debrecen H-4001, Hungary*

[6]*Department of Physics, University of Douala, P.O. Box 24157, Douala, Cameroon*

[7]*Max-Planck-Institut für Kernphysik, Saupfercheckweg 1, Heidelberg D-69117, Germany*

(Received 12 November 2012; published 6 February 2013)

Our approach to the dissociative recombination and competitive processes based on the multichannel quantum defect theory is extended to the full account of the dissociative excitation, including the electronic excitation of the molecular ion. Compared to other existing modelings, ours relies on a simpler and less-time-consuming discretization of the vibrational continua of the target ion and to a more accurate account of the Rydberg-valence interactions via a second-order solution of the Lippman-Schwinger equation. A thorough study of the competition among the dissociative recombination, vibrational excitation, and dissociative excitation is performed, including a detailed analysis of the two different mechanisms governing the ion dissociation. The application of our method to the high-energy electron collisions with H_2^+ and HD^+ ions results in a cross section in good agreement with the best previous modeling and with the most recent measurements performed in the Test Storage Ring of the Max-Planck-Institut für Kernphysik in Heidelberg.

DOI: 10.1103/PhysRevA.87.022702 PACS number(s): 34.80.Gs, 34.80.Ht, 34.80.Lx

I. INTRODUCTION

Dissociative recombination (DR) of molecular cations with electrons [1] is one of the simplest paradigms for the reactive collisions and a major elementary process, driving the charged-particle densities in astrophysical ionized media, fusion plasmas in the divertor region, hypersonic entry plasmas, and in many other cold media of technological interest [2,3].

Within this paper, rotational structure and interactions are neglected and, consequently, the DR process writes

$$AB^+(v_i^+) + e^-(\varepsilon) \longrightarrow [A + B]_\epsilon. \tag{1}$$

This scheme is appropriate for diatomic systems but can be generalized for polyatomic ones. v_i^+ stands for the initial vibrational quantum number in the relevant modes of the target cation, considered in its ground electronic state, ε is the energy of the incident electron, whereas, ϵ is the relative kinetic-energy release of the products.

DR is competing with the elastic, inelastic, or superelastic electron scattering,

$$AB^+(v_i^+) + e^-(\varepsilon) \longrightarrow AB^+(v_f^+) + e^-(\varepsilon_f), \tag{2}$$

corresponding to ε_f equal, smaller, or larger than ε, respectively. These processes, consequences of the autoionization, are also very important for the chemistry and for the energetics of the molecular species in cold reactive media.

During the last 60 years, DR and its competitive processes have been the subject of an increasing number of experimental and theoretical papers. Indeed, the first robust modeling of the DR, based on the application of the configuration interaction method of Fano [4] to molecular processes, was that of Bardsley [5], who proposed two mechanisms, both assisted by the autoionization: the *direct* mechanism, consisting of the capture of the electron into a dissociative state, and the *indirect* mechanism, relying on the temporary capture of the electron into a bound (Rydberg) state of the neutral AB^*, subsequently predissociated by a repulsive state AB^{**}. In opposition to this, Giusti-Suzor [6] assumed that the two mechanisms *interfere* and applied the multichannel quantum defect theory (MQDT) [7–10], rather than the configuration interaction method [11].

At high energies, when ε exceeds the energy necessary to break up the target cation, electron impact ion dissociation, i.e., dissociative excitation (DE),

$$AB^+(v_i^+) + e^-(\varepsilon) \longrightarrow [A + B^+]_\epsilon + e^-(\varepsilon_f) \tag{3}$$

becomes possible and adds incoherently to the previous scattering processes (1) and (2), resulting most often in the decrease in the DR yield.

The purpose of this paper is to improve our MQDT treatment of the dissociative recombination by the account of the dissociative excitation in order to produce reliable high-energy DR cross sections.

The role of the DE on the DR has been addressed since 1995 for HD^+ [12–14]. Our initial approach [13,14] has been restricted to a first-order account of the break up of the target via the vibrational continuum of its electronic ground state—a process which we call DE of the first kind (DE1)—and relied on the inclusion of this continuum in the survival factor (cf. Eq. (A5) in Ref. [6]).

A more rigorous account of DE was eventually given by Takagi [15]. He divided the continuum part of the vibrational spectrum in narrow energy bands and, integrating the energy-normalized wave function between their borders,

he discretized this continuum. This allowed treating the DE process [Eq. (3)] as vibrational excitation [Eq. (2)]. He also addressed the problem of the DE via excited electronic states of the cation—a process which we may call DE of the second kind (DE2)—completing an efficient approach which, from then on, could provide correct DR and DE cross sections at high energies. However, within his approach, the Rydberg-valence interaction was computed in the first order only.

Inspired by the seminal work of Takagi [15], we have built our own theoretical and numerical method, resulting, in a first stage in DE1 evaluations for HD^+ and DT^+ [16,17] within a collaboration with a group from Bucharest University. When DE2 was included in our formalism, this latter group decided to split and to publish, on their own, a series of results [18].

The purpose of the present paper is to provide an improved theoretical and numerical method for the study of the DR at high energies in comparison with Takagi [15] and Stroe and Fifirig [18]. It relies on an alternative discretization technique of the vibrational continua of the target ion and on a more accurate account of the Rydberg-valence interactions. More specifically, we elaborated a rigorous second-order approach of the reactive electron-molecular cation collisions, avoiding the serious inconsistencies in solving the Lippman-Schwinger equation in the same interaction region as in Ref. [18] and providing a more-detailed characterization of the two distinct processes DE1 and DE2.

Our paper is organized as follows: The main elements of our low-energy approach of the DR are summarized in Sec. II. The extension of our method by the inclusion of DE is the subject of Sec. III. Section IV is devoted to the illustration of the competition among dissociative recombination, vibrational excitation, and dissociative excitation. Our main results and their comparison with the experimental and the best theoretical results are presented in Sec. V. Section VI provides our conclusions. An extensive appendix illustrates the solution of the Lippman-Schwinger equation, generalized to the case of the DE inclusion.

II. THE MQDT-TYPE APPROACH TO THE LOW-ENERGY DISSOCIATIVE RECOMBINATION

A. The relevant states and channels

In this section, we restrict ourselves to the case where the energy of the incident electron prevents reaching the dissociation threshold of the ion in the ground electronic state. Consequently, the processes described in Eqs. (1) and (2) lead to the formation of intermediate collision complexes whose properties actually determine their final outcome. The account of these states allows the writing of the preceding reactions in the more explicit form

$$AB^+(v_i^+) + e^-(\varepsilon) \rightarrow AB^{*(c)}, AB^{**}, AB^* \rightarrow \begin{cases} [A+B]_\epsilon, \\ AB^+(v_f^+) + e^-(\varepsilon_f), \end{cases} \tag{4}$$

in which $AB^{*(c)}$ stands for states from the monoelectronic *ionization* continuum but bound from the vibrational point of view, AB^{**} stands for states from the vibrational continuum—i.e., dissociative—but bound from the electronic point of view, and AB^* stands for states both electronically and vibrationally bound.

The occurrence of the AB^* states, often called "Rydberg resonances," is the main reason for building an approach of the DR [5,6] based on the MQDT [7–10].

The processes (4) result from the coupling between ionization and dissociation channels, i.e., groups of states characterized by a common set of quantum numbers and by the same fragmentation threshold (either for ionization or for dissociation), having the energy below or above this threshold. More specifically, within a *quasidiabatic* representation [5,6,19], an *ionization* channel is built starting from the ground electronic state of the ion in one of its vibrational levels v^+—which we call "core 1"—and is completed by gathering all the monoelectronic states of a given orbital quantum number l, describing an "optical" electron. These monoelectronic states describe, with respect to the v^+ threshold, either a "free" electron—in which case the total state $AB^{*(c)}$ corresponds to (auto)ionization—or a bound electron—in which case the total state AB^* corresponds to a temporary capture into a Rydberg state. Meanwhile, a dissociation channel relies on an electronically bound state AB^{**} whose potential energy in the asymptotic limit is situated below the total energy of the system. Accordingly, the ionization channels gather together AB^* and $AB^{*(c)}$ states, and the dissociation channels correspond to AB^{**} states.

Given the total energy of the molecular system, a channel is *open* if this energy is higher than the energy of its fragmentation threshold and is *closed* in the opposite case.

In order to simplify the equations appearing in Sec. III, we restrict our discussions and derivations in Secs. II–IV and in the Appendix to the case where only one single partial wave of the Rydberg electron in an ionization channel is available. In the following, we omit the dependence on the orbital quantum number l unless it is specifically required. The generalization of these equations to the case of further partial waves is straightforward, and our present calculations (corresponding to the results in Sec. V) involve two partial waves for one of the relevant symmetries, namely, $^1\Sigma_g^+$.

B. Interactions in the reaction region

The MQDT approach starts with the building of the interaction matrix $\boldsymbol{V}$, performed in the A region [20] where the Born-Oppenheimer context is appropriate for the description of the collision system.

For a given symmetry Λ (quantum number related to the projection of the total electronic orbital angular momentum on the internuclear axis), the states belonging to an ionization channel may be modeled reasonably well with respect to hydrogenic states in terms of the quantum defect $\mu^\Lambda(R)$, which is dependent on the internuclear distance R, but is assumed to be independent of energy. An ionization channel of core 1, labeled by v—vibrational quantum number of a Rydberg state—rather than v^+—standing for a vibrational quantum number of the ion core—can be coupled to a dissociation channel, labeled d_j, on the electronic level first, through an R-dependent scaled Rydberg-valence interaction term $\mathcal{V}_{d_j}^{(e)\Lambda}(R)$, which is assumed to be independent of the energy of the electronic state.

This is the only possible interchannel electronic coupling, and by integrating these couplings over the internuclear distance, the nonvanishing elements of the interaction matrix $\boldsymbol{V}$ is as follows:

$$V^{\Lambda}_{d_j,v}(E,E') = \left\langle F^{\Lambda}_{d_j} \middle| \mathcal{V}^{(e)\Lambda}_{d_j}(R) \middle| \chi^{\Lambda}_{v} \right\rangle. \tag{5}$$

Here, χ^{Λ}_{v} is the vibrational wave function associated with an ionization channel in the interaction (i.e., the A) region, and $F^{\Lambda}_{d_j}$ is the radial wave function of a dissociative state d_j of symmetry Λ.

Starting from the interaction matrix $\boldsymbol{V}$ and from the zero-order Hamiltonian $\boldsymbol{H_0}$, (diagonal in both the ionization and the dissociation channel's representations), we build the reaction matrix $\boldsymbol{\mathcal{K}}$, which satisfies the Lippmann-Schwinger equation,

$$\boldsymbol{\mathcal{K}} = \boldsymbol{V} + \boldsymbol{V}\frac{\mathbf{1}}{E - \boldsymbol{H}_0}\boldsymbol{\mathcal{K}}. \tag{6}$$

This can be solved perturbatively. However, in a previous paper [21], we have shown that when the Rydberg-valence interactions $\mathcal{V}^{(e)\Lambda}_{d_j}$ do not depend on the energy of the Rydberg electron as we assume presently, Eq. (6) can be solved exactly in the second order.

In order to express the effects of the short-range interaction in terms of phase shifts, we perform a unitary transformation of our initial basis into a new one, corresponding to eigenchannels [6] via the diagonalization of the reaction matrix $\boldsymbol{\mathcal{K}}$,

$$\boldsymbol{\mathcal{K}}\boldsymbol{\mathcal{U}} = -\frac{1}{\pi}\mathbf{tan}(\boldsymbol{\eta})\boldsymbol{\mathcal{U}}, \tag{7}$$

where $\boldsymbol{\mathcal{U}}$ is a matrix whose columns are the eigenvectors and the diagonal matrix $\mathbf{tan}(\boldsymbol{\eta})$ contains the eigenvalues.

C. Dynamics in the outer region: The calculation of the cross section

In the external "B region" [20], the Born-Oppenheimer representation is no longer valid for the neutral molecule, and a frame transformation into the close-coupling representation [12,22,23] is performed via the projection coefficients,

$$\mathcal{C}_{v^+,\Lambda\alpha} = \sum_{v} U^{\Lambda}_{v,\alpha} \langle \chi_{v^+}(R) | \cos\left[\pi\mu^{\Lambda}(R) + \eta^{\Lambda}_{\alpha}\right] | \chi_v(R) \rangle, \tag{8}$$

and

$$\mathcal{C}_{d,\Lambda\alpha} = U^{\Lambda}_{d\alpha} \cos\,\eta^{\Lambda}_{\alpha}. \tag{9}$$

These can be organized in a matrix $\boldsymbol{\mathcal{C}}$. On the other hand, the coefficients $\mathcal{S}_{v^+,\Lambda\alpha}$ and $\mathcal{S}_{d_j,\Lambda\alpha}$ are obtained by replacing the cosine with the sine in Eqs. (8) and (9) and generate the matrix $\boldsymbol{\mathcal{S}}$.

$\boldsymbol{\mathcal{C}}$ and $\boldsymbol{\mathcal{S}}$ are the building blocks of the generalized scattering matrix $\boldsymbol{X}$, involving all the channels, open ("o") and closed ("c"), and organized in four submatrices,

$$\boldsymbol{X} = \frac{\boldsymbol{\mathcal{C}} + i\boldsymbol{\mathcal{S}}}{\boldsymbol{\mathcal{C}} - i\boldsymbol{\mathcal{S}}} = \begin{pmatrix} \boldsymbol{X}_{oo} & \boldsymbol{X}_{oc} \\ \boldsymbol{X}_{co} & \boldsymbol{X}_{cc} \end{pmatrix}. \tag{10}$$

Imposing boundary conditions leads to the physical scattering matrix [7],

$$\boldsymbol{S} = \boldsymbol{X}_{oo} - \boldsymbol{X}_{oc}\frac{1}{\boldsymbol{X}_{cc} - \exp(-i2\pi\boldsymbol{\nu})}\boldsymbol{X}_{co}, \tag{11}$$

where the diagonal matrix $\boldsymbol{\nu}$ is formed with the effective quantum numbers $\nu_{v^+} = [2(E_{v^+} - E)]^{-1/2}$ (in atomic units) associated with each vibrational threshold E_{v^+} of the ion situated above the current total energy E (and, consequently, labeling a closed channel).

For a molecular ion, initially on the level v_i^+ recombining with an electron of energy ε, the cross section of capture into all the dissociative states d_j of the same symmetry "sym" [gerade (ungerade), singlet (triplet)] and electronic angular momentum projection Λ can be written as

$$\sigma^{\mathrm{sym},\Lambda}_{\mathrm{diss}\leftarrow v_i^+} = \frac{\pi}{4\varepsilon}\rho^{\mathrm{sym},\Lambda}\sum_{j}\left|S_{d_j,v_i^+}\right|^2, \tag{12}$$

whereas, the total cross section for DR is obtained by summing over all available Λ's,

$$\sigma^{\mathrm{sym}}_{\mathrm{diss}\leftarrow v_i^+} = \sum_{\Lambda}\sigma^{\mathrm{sym},\Lambda}_{\mathrm{diss}\leftarrow v_i^+}. \tag{13}$$

Here, $\rho^{\mathrm{sym},\Lambda}$ is the ratio between the spin multiplicities of the neutral and the target ion.

Similarly, the total cross section for vibrational excitation from the initial vibrational state v_i^+ into the state v_f^+ writes

$$\sigma^{\mathrm{sym}}_{v_f^+\leftarrow v_i^+} = \sum_{\Lambda}\sigma^{\mathrm{sym},\Lambda}_{v_f^+\leftarrow v_i^+}, \tag{14}$$

where

$$\sigma^{\mathrm{sym},\Lambda}_{v_f^+\leftarrow v_i^+} = \frac{\pi}{4\varepsilon}\rho^{\mathrm{sym},\Lambda}\left|S_{v_f^+,v_i^+}\right|^2. \tag{15}$$

III. EXTENSION OF OUR THEORETICAL APPROACH TO THE HIGH-ENERGY DISSOCIATIVE RECOMBINATION: THE ROLE OF THE DISSOCIATIVE EXCITATION

A. The states and channels related to the vibrational continua of the ion

At energies higher than the dissociation threshold of the ion, we have to take into account the autoionization resulting into states from the continuum part of the vibrational spectrum, i.e., *dissociative excitation* [DE, Eq. (3)]. In terms of resonant states involved and the competition between the different exit channels, this corresponds to the replacement of Eq. (4) with the following:

$$AB^+(v_i^+) + e^-(\varepsilon) \rightarrow AB^{*(c)}, AB^{**}, AB^{**(c)} \rightarrow \begin{cases} [A+B]_{\epsilon}, \\ AB^+(v_f^+) + e^-(\varepsilon_f), \\ [A+B^+]_{\epsilon'} + e^-(\varepsilon_f), \end{cases} \tag{16}$$

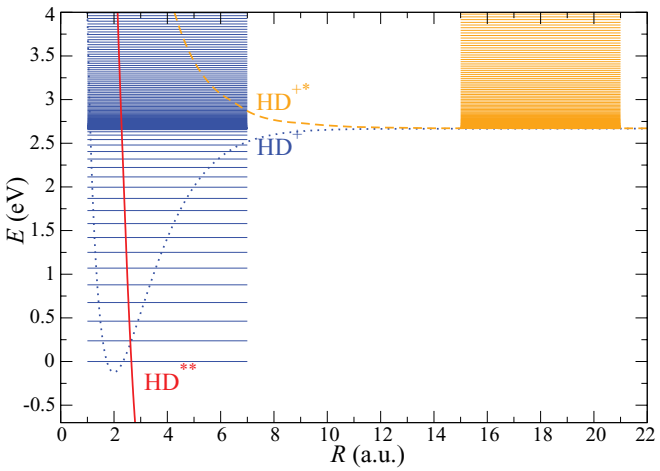

FIG. 1. (Color online) HD^+-HD states relevant for the electron-HD^+ reactive collisions. Potential-energy curves for dotted curve (blue): $HD^{+2}\Sigma_g^+(1s\sigma_g)$; dashed curve (orange) $HD^{+2}\Sigma_u^+(2p\sigma_u)$; solid line (red): $HD^{**1}\Sigma_g^+(2p\sigma_u^2)$ dissociative states. The vibrational levels relying on the ground and excited cores are represented by horizontal thin lines, colored blue and orange, respectively.

where AB^* has been removed (since all the bound ionization channels are open and the capture into Rydberg states is excluded) and $AB^{**(c)}$ has been added, labeling dissociative states from the monoelectronic continuum. These states, representing a free electron in the field of a dissociating ion, can be organized either into dissociation channels or into ionization ones, but the latter option has been preferred so far. In order to be explicit on the developments that we implemented, we refer concretely to the case of H_2 and HD systems.

The $AB^{**(c)}$ states invoked above are, in this case, built on two electronic states of the ionic cores, the $^2\Sigma_g^+(1s\sigma_g)$—referred to as core 1—dotted (blue) potential-energy curve (PEC) and $^2\Sigma_u^+(2p\sigma_u)$—referred to as core 2—dashed (orange) PEC in Fig. 1. We have discretized their vibrational continua by providing a wall of 15 eV height at $R = 25$ a.u. [10] (1 a.u. $= a_0 = 0.052\,9177$ nm). This corresponds, for every partial wave of the incident electron, to about 334 and 291 further ionization channels for the ground cores of HD^+ and $H_2{}^+$, respectively—responsible for DE1—and to 383 and 375 ionization channels for the excited cores of HD^+ and $H_2{}^+$, respectively—responsible for DE2.

Finally, since the temporary capture into bound Rydberg states AB^* is excluded above the dissociation limit of the ion PEC, the collision process is exclusively driven by the direct mechanism.

B. Further interactions implied by the dissociative excitation in the reaction region

When dissociative excitation is included in our approach, the coupling between a given dissociation channel d_j and an ionization one v, built on core 1—Eq. (5)—is extended to the continuum part of the vibrational spectrum (previously discretized as shown in the preceding subsection).

On the other hand, every channel v is coupled to the further ionization channels built on core 2, labeled generically by w.

These couplings are quantified at the electronic level by the R-dependent interaction term $\tilde{\mathcal{V}}^{(e)\Lambda}(R)$—assumed to be energy independent—and they have the following form:

$$V_{wv}^{\Lambda}(E,E') = \left\langle \chi_w^{\Lambda} \middle| \tilde{\mathcal{V}}^{(e)\Lambda}(R) \middle| \chi_v^{\Lambda} \right\rangle. \tag{17}$$

Besides the elements given by Eqs. (5) and (17) in which v and w span, for every Λ symmetry, *all* the available vibrational levels (bound and discretized continua), the remaining elements of the interaction matrix—$V_{d_i d_j}^{\Lambda}$, $V_{d_i w}^{\Lambda}$, $V_{vv'}^{\Lambda}$, and $V_{ww'}^{\Lambda}$—vanish, since in the quasidiabatic representation chosen here, they concern pairs of channels associated with the same ionic core [19].

Consequently, the actual reaction matrix in block form is as follows:

$$\mathcal{K} = \begin{pmatrix} \mathcal{K}_{\bar{d}\bar{d}} & \mathcal{K}_{\bar{d}\bar{v}} & \mathcal{K}_{\bar{d}\bar{w}} \\ \mathcal{K}_{\bar{v}\bar{d}} & \mathcal{K}_{\bar{v}\bar{v}} & \mathcal{K}_{\bar{v}\bar{w}} \\ \mathcal{K}_{\bar{w}\bar{d}} & \mathcal{K}_{\bar{w}\bar{v}} & \mathcal{K}_{\bar{w}\bar{w}} \end{pmatrix}, \tag{18}$$

where the *collective* indices $\bar{d}$, $\bar{v}$, and $\bar{w}$ in Eq. (18) span the ensembles of all the available individual ones and d_j, v, and w are labeling dissociation channels, ionization channels built on core 1, and ionization channels built on core 2, respectively. Whereas, the matrix formed by the first two rows and columns stand for the DR at low energies, the third row and the third column complete the reaction matrix for the correct description of the DR at high energies, including the DE.

As in the case of DR at low energy (Sec. II), the Lippmann-Schwinger equation can be solved exactly in second order when the interactions $\mathcal{V}_{d_j}^{(e)\Lambda}$ and $\tilde{\mathcal{V}}^{(e)\Lambda}$ do not depend on the energy of the incident electron. Whereas, the first-order solution of Eq. (6) accounts for the electronic coupling between ionization and dissociation channels, the second-order one goes further in accuracy, accounting for electronic coupling between ionization channels, an aspect which was not addressed in the previous papers [15,18]. The derivation of this solution for the DE-assisted DR is given in full detail in the Appendix, which is a thorough quantitative analysis of the interactions brought by the DE. We outline here only the output of this derivation.

The nonvanishing elements for all the allowed d_i, d_j, v, v', w, and w' dissociation and ionization channels are as follows:

$$K_{vd_j}^{\Lambda} = K_{d_j v}^{\Lambda} = V_{vd_j}^{\Lambda}, \tag{19}$$

$$K_{vw}^{\Lambda} = K_{wv}^{\Lambda} = V_{vw}^{\Lambda}, \tag{20}$$

$$K_{vv'}^{\Lambda} = \frac{1}{W} \iint \left[\chi_v^{\Lambda}(R) \mathcal{V}_{d_j}^{(e)\Lambda}(R) F_d^{\Lambda}(R_<) \times G_d^{\Lambda}(R_>) \mathcal{V}_{d_j}^{(e)\Lambda}(R') \chi_{v'}^{\Lambda}(R') \right] dR\, dR'. \tag{21}$$

In Eq. (20), W denotes the Wronskian of the regular (F_d) and the irregular (G_d) solution of the dissociative state nuclear Schrödinger equation. Due to the previously explained reasons, all the other elements will vanish, namely,

$$K_{d_i d_j} = 0, \quad K_{d_i w} = K_{w d_j} = 0, \quad K_{ww'} = 0. \tag{22}$$

Taking all of these into account, the second-order reaction matrix has the form

$$\mathcal{K} = \begin{pmatrix} \mathbf{O} & \boldsymbol{V}_{\bar{d}\bar{v}} & \mathbf{O} \\ \boldsymbol{V}_{\bar{v}\bar{d}} & \mathcal{K}_{\bar{v}\bar{v}} & \boldsymbol{V}_{\bar{v}\bar{w}} \\ \mathbf{O} & \boldsymbol{V}_{\bar{w}\bar{v}} & \mathbf{O} \end{pmatrix}, \tag{23}$$

where the elements of each block are given by Eqs. (5), (17), and (20) and $\mathbf{O}$ is the null matrix.

C. Dissociative recombination and excitation dynamics: The calculation of the cross section

The inclusion of dissociative excitation due to the presence of the discretized continuum levels of the two cores increases not only the dimension of the interaction matrix $\boldsymbol{V}$ [Eq. (17)] and the reaction matrix (18), but also that of the frame transformation $\boldsymbol{\mathcal{C}}$ and $\boldsymbol{\mathcal{S}}$ matrices. Consequently, the sum on the right-hand side of Eq. (8) is extended to the quasicontinuum levels, and further matrix elements, corresponding to the quasicontinuum levels of the second core (w), occur.

The $\boldsymbol{X}$ matrix and, finally, the $\boldsymbol{S}$ matrix are eventually built according to Eqs. (10) and (11), respectively. The DE1 and DE2 processes are actually treated as vibrational excitations from an initial vibrational state v_i^+ to the (discretized) ionization continua of the two cores. The cross sections for these processes are given by

$$\sigma^{\mathrm{sym},\Lambda}_{\mathrm{DE1},v_i^+} = \frac{\pi}{4\varepsilon}\rho^{\mathrm{sym},\Lambda} \sum_{v_h^+ < v^+ < v^+_{\max}(\varepsilon)} \left|S_{v^+,v_i^+}\right|^2, \tag{24}$$

and

$$\sigma^{\mathrm{sym},\Lambda}_{\mathrm{DE2},v_i^+} = \frac{\pi}{4\varepsilon}\rho^{\mathrm{sym},\Lambda} \sum_{w^+ < w^+_{\max}(\varepsilon)} \left|S_{w^+,v_i^+}\right|^2. \tag{25}$$

The total DE cross section has the form

$$\sigma_{\mathrm{DE},v_i^+} = \sum_{\mathrm{sym},\Lambda} \sigma^{\mathrm{sym},\Lambda}_{\mathrm{DE},v_i^+}, \tag{26}$$

where

$$\sigma^{\mathrm{sym},\Lambda}_{\mathrm{DE},v_i^+} = \sigma^{\mathrm{sym},\Lambda}_{\mathrm{DE1},v_i^+} + \sigma^{\mathrm{sym},\Lambda}_{\mathrm{DE2},v_i^+}. \tag{27}$$

v_h^+ is the highest *bound* vibrational level built on core 1, whereas, $v^+_{\max}(\varepsilon)$ and $w^+_{\max}(\varepsilon)$ are the highest quasicontinuum vibrational levels situated below the current total energy $E = E_{v_i^+} + \varepsilon$, corresponding to core 1 and core 2, respectively.

IV. ILLUSTRATIONS OF THE COMPETITION BETWEEN THE RELEVANT SIMULTANEOUS PROCESSES

In order to distinguish between the two types of excitations—vibrational and dissociative—and to understand the intimate link between them, we will explore a broad energy range, from zero to energies above the dissociation energy of the ion (2.67 eV).

To simplify our analysis, we neglect the *indirect* mechanism in the low-energy region and restrict ourselves to the *open* channels, i.e., accounting for the *direct* process only. Consequently, the $\boldsymbol{X}$ matrix from Eq. (10) reduces to its $\boldsymbol{X}_{oo}$ component, and all the resonant parts from the second term of the $\boldsymbol{S}$ matrix in Eq. (11) are missing.

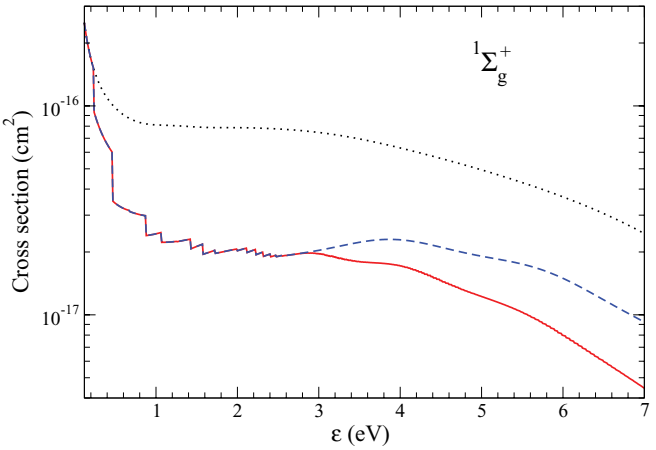

FIG. 2. (Color online) Direct dissociative recombination of the ground-state HD^+ ion with a d ($l = 2$) electron into the lowest $^1\Sigma_g^+(2p\sigma_u)^2$ HD^{**} state. Dotted black curve: only $v^+ = v_i^+ = 0$ included in the calculation. Dashed (blue) curve: all bound vibrational levels ($v^+ = 0$–20) are included. Solid (red) curve: bound vibrational levels and discretized vibrational levels from the continuum of the ground-state ion (dissociative excitation of the first kind) are included.

Figure 2 displays the cross section for the DR of a ground-state HD^+ ($v_i^+ = 0$) ion with a d ($l = 2$) electron into the lowest $^1\Sigma_g^+(2p\sigma_u)^2$ HD^{**} dissociative state in three cases: the entrance ionization channel—corresponding to the ground vibrational state of the ion—available only (dotted black curve), all the ionization channels corresponding to the bound vibrational state of the ion available [dashed (blue) curve], and all the ionization channels built on bound *and* quasicontinuum vibrational levels available [solid (red) curve].

Although the results in Fig. 2 come from the full MQDT calculations as those described in the preceding section, in order to get a better insight into the mechanisms illustrated there, we recall a simple model, qualitatively appropriate in our case, based on the following approximations:

(i) The first-order solution of the Lippman-Schwinger equation (6) is adopted, and

(ii) the R dependence of the quantum defects is neglected.

Within these assumptions, the direct DR cross section can be written as a product of a capture cross section σ_{cap} and a "survival" factor f_{surv} [6],

$$\sigma^{\mathrm{sym},\Lambda}_{\mathrm{diss}\leftarrow v_i^+} = \sigma_{\mathrm{cap}} f_{\mathrm{surv}}, \tag{28}$$

where

$$\sigma_{\mathrm{cap}} = \frac{\pi}{\varepsilon}\rho^{\mathrm{sym},\Lambda}\xi^2_{v_i}, \tag{29}$$

and

$$f_{\mathrm{surv}} = \frac{1}{\left[1 + \sum_{v_{\mathrm{open}}} \xi_v^2\right]^2}. \tag{30}$$

All these quantities rely on the strength of the Rydberg-valence interaction,

$$\xi_v = \pi V^{\Lambda}_{dv}. \tag{31}$$

The simplest case in Fig. 2 comes from the account of one single ionization channel, the entrance one. Here, DR is in competition with the elastic scattering only, and according to

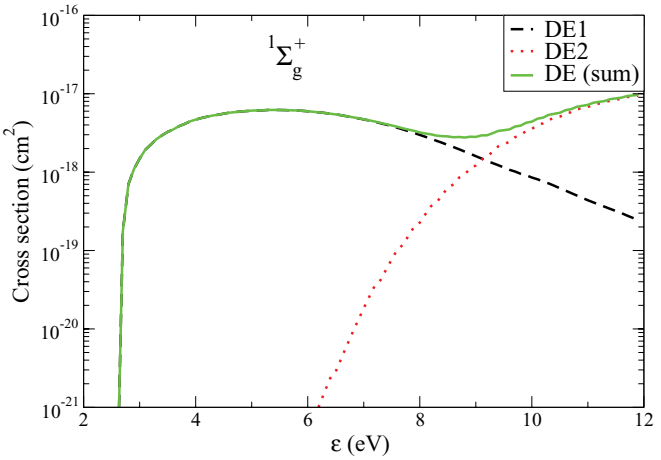

FIG. 3. (Color online) DE1 and DE2 cross sections for the HD^+ ground-state ion on impact with electrons. The contribution of the lowest dissociative state of the $^1\Sigma_g^+$ symmetry and of the $l = 2$ partial wave of the Rydberg electron is illustrated, the calculations having been performed in the second order of the reaction matrix. The solid (green) line stands for the total DE cross section, whereas, the dashed black and dotted red lines illustrate the the DE1 and DE2 cross sections, respectively.

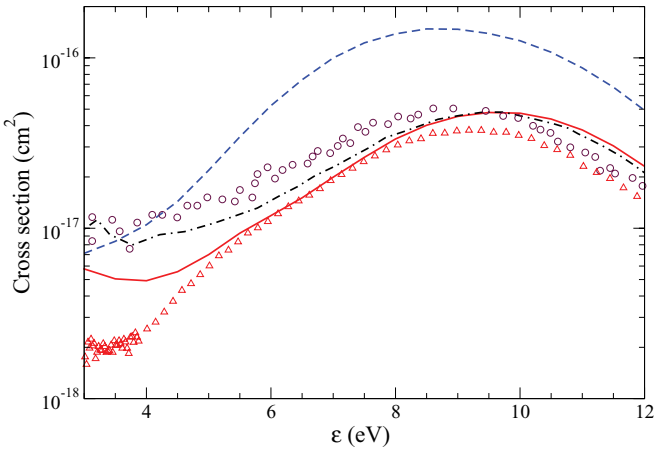

FIG. 4. (Color online) Dissociative recombination of the ground state of the HD^+ ion, global cross sections. Dashed blue (solid red) curves: second-order calculations with dissociative excitation neglected (accounted). Black dot-dashed curve: computation of Takagi [15]. Circles: measurements of Tanabe *et al.* [12]. Triangles: measurements representing the Heidelberg data in Al-Khalili *et al.* [24].

the preceding equations, one finds the cross section given by the smooth dotted black curve.

In the second case, we involve further ionization channels, namely, those associated with the *bound* vibrational levels, which mean that we allow for more autoionization through vibrational excitation. At very low energy, the cross section—the dashed (blue) curve in Fig. 2—evolves smoothly and is identical to that from the first case. However, when the energy rises, it drops suddenly as each new vibrational threshold opens in agreement with the simple predictive equations (28)–(31). When the last vibrational bound level is reached ($v^+ = 20$), the cross section continues to decrease without displaying any further steplike structure. Notice that autoionization through vibrational excitation results in the decrease in the DR cross section by a factor of up to 5 with respect to the first case discussed.

Finally, at energies higher than the dissociation threshold of the ion as shown in Sec. III, the vibrational excitation continues to compete with the dissociative recombination but becomes richer, being extended to dissociative excitation. The solid (red) curve in Fig. 2 represents the cross section of DR assisted by DE1 only and shows that this latter process decreases the DR with respect to that affected by vibrational excitation only [dashed (blue) curve] by a factor up to 2.

As for the DE2 process, it is completely negligible at low energies, but it becomes dominant above 10 eV as Fig. 3 illustrates for the case of the HD^+-HD system.

V. RESULTS FOR THE DISSOCIATIVE RECOMBINATION OF BENCHMARK CATIONS: HD^+ AND H_2^+

The most-recent high-energy experiments devoted to the benchmark diatomic hydrogen cation have been performed on HD^+ in Heidelberg, Stockholm, Aarhus [24], and Tokyo [12]. Therefore, we have performed extensive calculations on this hydrogen isotopolog: We have computed the DE-assisted DR cross section for capture into all the dissociative states within every relevant symmetry $^1\Sigma_g^+$, $^{1,3}\Sigma_u^+$, $^{1,3}\Pi_{u,g}$, and for a broad range of energies, i.e., between the dissociation thresholds—2.67 and 12 eV. The results are shown in Fig. 4.

These calculations have been carried out using the first order and, alternatively, the second order of the solution of the Lippman-Schwinger equation for the reaction matrix [Eq. (6) and the Appendix] and have relied on molecular data previously used [25–27]. Our most accurate cross section, i.e., the solid (red) curve in Fig. 4, is in better agreement with the most recent measurements [24] than the previous theoretical estimations [15] below 8 eV. One may notice the huge effect of the dissociative excitation, which when taken into account in the theoretical modeling, makes the dissociative recombination cross section decrease by a factor up to 4 around 7 eV.

Significant structures due to the opening of the final channels with D ($n \geqslant 3$) or H ($n \geqslant 3$) have already been

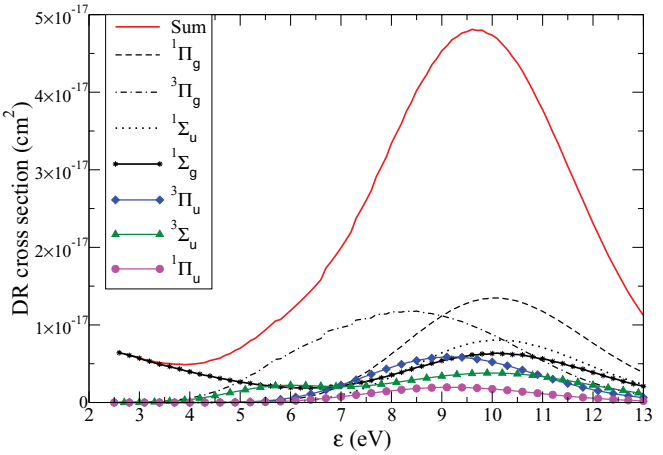

FIG. 5. (Color online) Dissociative recombination of the ground-state HD^+ ion, contributions from each symmetry (indicated in the panel) to the global DR cross section.

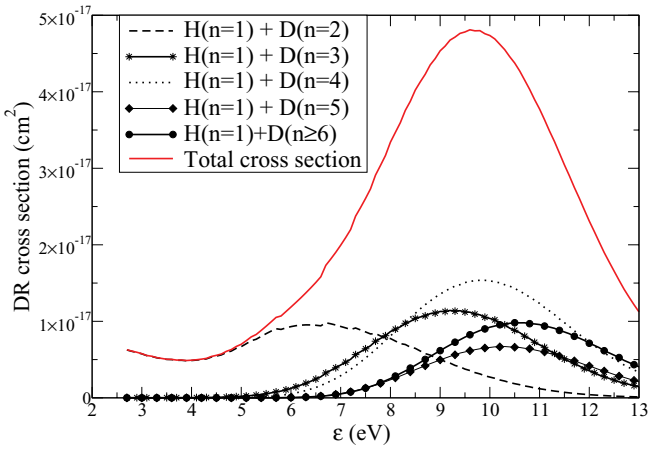

FIG. 6. (Color online) Dissociative recombination of the ground-state HD^+ ion, contributions of each pair of atomic states resulting from dissociation. "H ($n = 1$) + D ($n = 2,3,4, \ldots$)" stands for "D ($n = 1$) + H ($n = 2,3,4, \ldots$)" too.

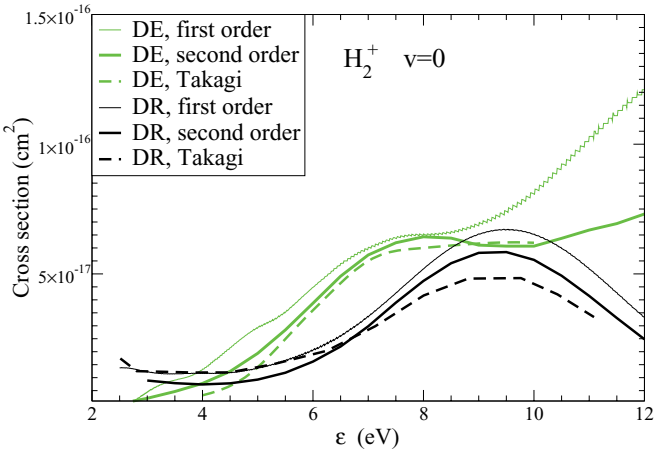

FIG. 8. (Color online) Dissociative recombination—black curves—and dissociative excitation—lighter (green) curves—of the H_2^+ molecular ion. Thin (thick) solid curves: first-order (second-order) calculations. Dashed curves: theoretical results of Takagi [15].

experimentally found at energies between 1 and 3 eV [28]. These structures represent the DR via the vibrational continuum of the monoexcited molecular Rydberg states. It should be noted that such processes can both increase and decrease the DR rate since the multiple crossings involved can open additional pathways both for autoionization (reducing the effective survival factor) and towards the atomic final states (increasing the rate of DR yielding excited atoms) [28]. Such processes, where dynamical transitions occur from the doubly excited dissociative states to monoexcited Rydberg states via a multitude of curve crossings, are not included in the present calculation since we focus on the high-energy region ($\varepsilon > 3$ eV).

Figure 5 provides the contributions of each of the seven symmetries considered in our analysis—all Σ and Π, gerade and ungerade, singlet and triplet symmetries, except the $^3\Sigma_g^+$ characterized by a negligible Rydberg-valence coupling. Whereas, the $^1\Sigma_g^+$ symmetry dominates below 5 eV, $^3\Pi_g$ is the most important above this energy and diminishes in favor of $^1\Pi_g$ above 9 eV.

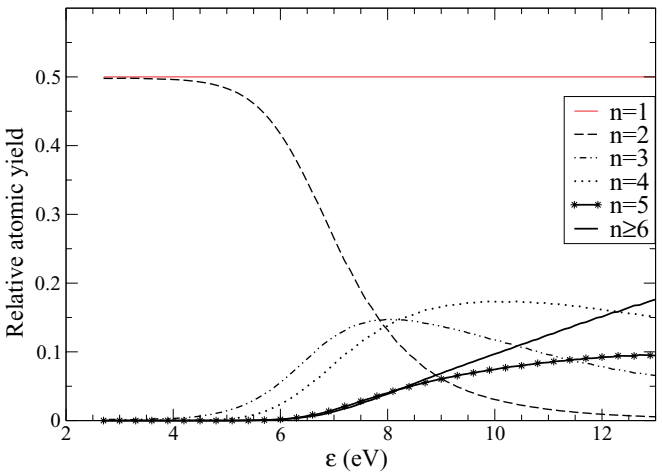

FIG. 7. (Color online) Dissociative recombination of the ground-state HD^+ ion, relative atomic H(n), or D(n) final-state yields.

Figures 6 and 7 provide the branching ratios and the relative atomic yields, respectively, assuming that no redistribution of the capture flux is effective at large internuclear distances via interactions with highly excited Rydberg states. Besides the atomic $n = 1$ ground state, the excited atomic states $n =$ 2–5 are dominantly populated around 6, 9, 10, and 12 eV, respectively.

Since the measurements on H_2^+ are not vibrationally resolved [29,30], we have compared our cross sections for this isotopolog with the best-available theoretical data. Figure 8 displays a good agreement between our results and those of Takagi [15], both for dissociative recombination and dissociative excitation. The cross sections of Takagi, computed within the first order of the reaction matrix, are smaller than our first-order ones, probably due to the different modalities in managing the very highly excited dissociative states and of their coupling with the ionization. One may also notice the huge importance of the electronic couplings between the ionization channels in the case of the dissociative excitation, illustrated by the notable difference at high energies between the second-order and the first-order cross sections.

VI. CONCLUSION

We have extended our approach of dissociative recombination in order to fully include its competition with dissociative excitation. This was achieved by extending our collision formalism to the case of two active electronic states of the cation by discretizing, in a simple and efficient way, the corresponding vibrational continua and by a complete inclusion of the relevant interactions via a rigorous derivation of the reaction matrix in the second order. The computed cross sections for the HD^+-HD system agree better than the previous modelings with the most recent storage ring measurements.

In the present paper, we focused on the role of competition of the dissociative excitation with respect to the dissociative recombination. However, we also performed preliminary computations of the dissociative excitation cross section itself for H_2^+, which proved to agree well with previous theoretical

estimations. A systematic series of further calculations are under way in order to provide extensive DE cross sections, which will be compared with the most recent, yet unpublished, measurements.

On the other hand, after having tested our approach by comparison with experiment and previous theory, we plan to perform more detailed DR and DE computations on isotopes of H_2^+ and major impurity hydride cations. This will provide new input data for the kinetic predictions of the hydrogen plasmas in the wall and divertor regions of the fusion devices, strongly needed in the present collisional-radiative models.

ACKNOWLEDGMENTS

The authors thank Ch. Jungen, J. Robert, H. Takagi, S. L. Guberman, M. Lange, H. Buhr, and X. Urbain for numerous and fruitful discussions. We acknowledge the scientific and financial support from the European Space Agency (Grant No. ESTEC 21790/08/NL/HE) and the International Atomic Energy Agency, (CRP "Light Element Atom, Molecule and Radical Behaviour in the Divertor and Edge Plasma Regions" and CRP "Atomic and Molecular Data for State-Resolved Modelling of Hydrogen and Helium and their isotopes in Fusion"). We have been supported by the French network "Fédération de Recherch Fusion Magnétique Controllée" (CEA, EFDA, and EURATOM), the ANR-contract "SUMOSTAI," and the CNRS/INSU programme "Physique et Chimie du Milieu Interstellaire." Financial support from Région Haute Normandie has been provided to us through the CPER (CNRT/"Energie, Electronique, Matériaux") and "Institut d'Energie, Fluides et Environnement" (Rouen-Le Havre). K.C. acknowledges financial support from the Conseil General de la Haute Normandie in the form of a postdoctoral fellowship under the People MCFR programme. J.Z.M. acknowledges financial support from Triangle de la Physique for postdoctoral grants and IFS Laboratoire Aimé Cotton for hospitality during his visit.

APPENDIX: THE REACTION MATRIX APPROPRIATE FOR THE MODELING OF HIGH-ENERGY DISSOCIATIVE RECOMBINATION AND DISSOCIATIVE EXCITATION

According to the Lippmann-Schwinger equation (6) in the energy representation, the elements of the reaction matrix for a given value of Λ—which are omitted in this Appendix for the sake of simplicity—write [21]

$$K_{ji}(E',E) = V_{ji}(E',E) + \sum_k \mathrm{P}\int dE'' \frac{V_{jk}(E',E'')K_{ki}(E'',E)}{E-E''}. \quad \text{(A1)}$$

Here, E, E', and E'' are the energies associated with the ionization or dissociation channels labeled by i, j, and k, and P refers to the principal value of the integral on the right-hand side.

The following specific indices are used:

(i) d: a dissociation channel.

(ii) $v/v'/v''$: an ionization channel associated with core 1.

(iii) $w/w'/w''$: an ionization channel associated with core 2.

As shown in Sec. III B as we restrict ourselves to the quasidiabatic representation, for all d_i, d_j, v, v', w, and w', we have

$$V_{d_i d_j} = 0, \quad V_{d_i w} = 0, \quad V_{vv'} = 0, \quad V_{ww'} = 0. \quad \text{(A2)}$$

As for the remaining interaction matrix elements, their properties rely on the assumption that the electronic couplings $\mathcal{V}_{d_j}^{(e)}(R)$ and $\tilde{\mathcal{V}}^{(e)}(R)$—introduced in Eqs. (5) and (17), respectively—are independent of the energy of the external electron in the involved ionization channels. This means that the dependence on energy comes from the *dissociative* channels only and, consequently,

$$V_{vd_j}(E',E) = V_{vd_j}(E), \quad \text{(A3)}$$

and

$$V_{vw}(E',E) = V_{vw}. \quad \text{(A4)}$$

In Eq. (A4), V_{vw} are independent of E' and E.

In block form, the reaction matrix has the structure given by Eq. (18).

In the first order, the reaction matrix is equal to the interaction matrix $\boldsymbol{V}$, introduced in Sec. II B and whose only nonvanishing matrix elements are those given by Eqs. (5) and (17).

From now on, we will focus on the second order $\boldsymbol{\mathcal{K}}^{(2)}$ of the reaction matrix (18) omitting the "$^{(2)}$" superscript for the sake of simplicity.

For any two dissociative channels d_1 and d_2, Eq. (6) implies

$$\begin{aligned} K_{d_1d_2}(E_1,E_2) &= V_{d_1d_2}(E_1,E_2) + \sum_{d_j} \mathrm{P}\int dE \frac{V_{d_1d_j}(E_1,E)K_{d_jd_2}(E,E_2)}{E_2-E} \\ &+ \sum_v \mathrm{P}\int dE' \frac{V_{d_1v}(E_1,E')K_{vd_2}(E',E_2)}{E_2-E'} \\ &+ \sum_w \mathrm{P}\int dE'' \frac{V_{d_1w}(E_1,E'')K_{wd_2}(E'',E_2)}{E_2-E''}. \end{aligned} \quad \text{(A5)}$$

Meanwhile, since $V_{d_1d_2} = V_{d_1w} = 0$ according to (A2), the above equation reduces to

$$K_{d_1d_2}(E_1,E_2) = \sum_v \mathrm{P}\int dE' \frac{V_{d_1v}(E_1,E')K_{vd_2}(E',E_2)}{E_2-E'}. \quad \text{(A6)}$$

In a similar way, for any two vibrational and dissociative channels w and d_1, respectively, Eq. (6) writes

$$\begin{aligned} K_{wd_1}(E'',E) &= V_{wd_1}(E'',E) + \sum_v \mathrm{P}\int dE' \frac{V_{wv}(E'',E')K_{vd_1}(E',E)}{E-E'} \\ &+ \sum_{w'} \mathrm{P}\int dE' \frac{V_{ww'}(E'',E')K_{w'd_1}(E',E)}{E-E'} \\ &+ \sum_{d_j} \mathrm{P}\int dE_j \frac{V_{wd_j}(E'',E_j)K_{d_jd_1}(E_j,E)}{E-E_j}. \end{aligned} \quad \text{(A7)}$$

Using Eqs. (A2) and (A4), Eq. (A7) becomes

$$K_{wd_1}(E'',E) = \sum_v V_{wv}\mathrm{P}\int dE' \frac{K_{vd_1}(E',E)}{E-E'}. \quad \text{(A8)}$$

The right-hand side of Eq. (A8) is independent of E'', and hence, we can write

$$K_{wd_1}(E'',E) = K_{wd_1}(E). \tag{A9}$$

Once we explored the blocks $\mathcal{K}_{\bar{d}\bar{d}}$ and $\mathcal{K}_{\bar{v}\bar{d}}$ of the reaction matrix (18), and now, we focus on the block $\mathcal{K}_{\bar{v}\bar{d}}$. For any two indices v,d_1,

$$\begin{aligned} K_{vd_1}(E',E) &= V_{vd_1}(E',E) + \sum_{v''} \mathrm{P}\int dE'' \frac{V_{vv''}(E',E'')K_{v''d_1}(E'',E)}{E-E''} \\ &+ \sum_{w} \mathrm{P}\int dE'' \frac{V_{vw}(E',E'')K_{wd_1}(E'',E)}{E-E''} \\ &+ \sum_{d_j} \mathrm{P}\int dE_1 \frac{V_{vd_j}(E',E_1)K_{d_jd_1}(E_1,E)}{E-E_1}. \end{aligned} \tag{A10}$$

The use of the third equation of (A2) and of (A3) reduces the above equation to

$$\begin{aligned} K_{vd_1}(E',E) = V_{vd_1}(E) &+ \sum_{w} V_{vw}\mathrm{P}\int dE'' \frac{K_{wd_1}(E'',E)}{E-E''} \\ &+ \sum_{d_j} \mathrm{P}\int dE_1 \frac{V_{vd_j}(E_1)K_{d_jd_1}(E_1,E)}{E-E_1}. \end{aligned} \tag{A11}$$

Furthermore, due to (A9), the first sum on the right-hand side of the above equation vanishes. Indeed,

$$\begin{aligned} &\sum_{w} V_{vw}\mathrm{P}\int dE'' \frac{K_{wd_1}(E'',E)}{E-E''} \\ &\quad = \sum_{w} V_{vw}K_{wd_1}(E)\mathrm{P}\int \frac{dE''}{E-E''} = 0, \end{aligned} \tag{A12}$$

as the principal part of the last integral is zero. Consequently, (A11) reduces to

$$K_{vd_1}(E',E) = V_{vd_1}(E) + \sum_{d_j} \mathrm{P}\int dE_1 \frac{V_{vd_j}(E_1)K_{d_jd_1}(E_1,E)}{E-E_1}. \tag{A13}$$

Noticing that Eq. (A13) does not depend on E', we may write

$$K_{vd_1}(E',E) = K_{vd_1}(E). \tag{A14}$$

Returning now to Eq. (A6) and using Eqs. (A3) and (A14), we find

$$K_{d_1d_2}(E_1,E_2) = \sum_{v} V_{d_1v}(E_1)K_{vd_2}(E_2)\mathrm{P}\int \frac{dE'}{E_2-E'} = 0 \tag{A15}$$

for all d_1,d_2.

Moreover, $K_{d_jd_1} = 0$ in Eq. (A13) implies

$$K_{vd_1}(E',E) = V_{vd_1}(E) \tag{A16}$$

for all v,d_1. Based on this latter result, Eq. (A8) becomes

$$K_{wd_1}(E'',E) = \sum_{v} V_{wv}V_{vd_1}(E)\mathrm{P}\int \frac{dE'}{E-E'} = 0 \tag{A17}$$

for all w,d_1.

We next calculate elements of the blocks $\mathcal{K}_{\bar{w}\bar{w}}$ and $\mathcal{K}_{\bar{v}\bar{w}}$. For any two indices w_1,w_2, we have

$$\begin{aligned} K_{ww'}(E,E') &= V_{ww'}(E,E') + \sum_{v} \mathrm{P}\int dE'' \frac{V_{wv}(E,E'')K_{vw'}(E'',E')}{E'-E''} \\ &+ \sum_{w''} \mathrm{P}\int dE'' \frac{V_{ww''}(E,E'')K_{w''w'}(E'',E')}{E'-E''} \\ &+ \sum_{d_j} \mathrm{P}\int dE_1 \frac{V_{wd_j}(E,E_1)K_{d_jw'}(E_1,E')}{E'-E_1}. \end{aligned} \tag{A18}$$

According to Eq. (A2), $V_{ww'} = V_{ww''} = V_{wd_j} = 0$. Consequently, (A18) reduces to

$$K_{ww'}(E,E') = \sum_{v} \mathrm{P}\int dE'' \frac{V_{wv}(E,E'')K_{vw'}(E'',E')}{E'-E''}. \tag{A19}$$

In order to evaluate $K_{vw'}(E'',E')$ in Eq. (A19), again, we use (A1),

$$\begin{aligned} K_{vw'}(E,E') &= V_{vw'}(E,E') + \sum_{v} \mathrm{P}\int dE'' \frac{V_{vv'}(E',E'')K_{v'w'}(E'',E')}{E'-E''} \\ &+ \sum_{w} \mathrm{P}\int dE'' \frac{V_{vw}(E,E'')K_{ww'}(E'',E')}{E'-E''} \\ &+ \sum_{d_j} \mathrm{P}\int dE_1 \frac{V_{vd_j}(E,E_1)K_{d_jw'}(E_1,E')}{E'-E_1}. \end{aligned} \tag{A20}$$

Making use of Eqs. (A2) and (A17) and the symmetry property of the reaction matrix together with Eq. (A4), the $K_{vw'}$ term will read as

$$K_{vw'}(E,E') = V_{vw'} + \sum_{w} V_{vw}\mathrm{P}\int dE'' \frac{K_{ww'}(E'',E')}{E'-E''}. \tag{A21}$$

Now, the right-hand side of Eq. (A21) is independent of E, so we can write

$$K_{vw'}(E,E') = K_{vw'}(E'). \tag{A22}$$

Using this and Eq. (A3), Eq. (A19) becomes

$$K_{ww'}(E,E') = \sum_{v} V_{wv}K_{vw'}(E')\mathrm{P}\int dE'' \frac{1}{E'-E''} = 0 \tag{A23}$$

for all w,w'.

Turning now to the elements of the block $\mathcal{K}_{\bar{v}\bar{w}}$, we have, for any v,w,

$$\begin{aligned} K_{vw}(E,E') &= V_{vw}(E,E') + \sum_{v'} \mathrm{P}\int dE'' \frac{V_{vv''}(E,E'')K_{v''w}(E'',E')}{E'-E''} \\ &+ \sum_{w'} \mathrm{P}\int dE'' \frac{V_{vw'}(E,E'')K_{w'w}(E'',E'')}{E'-E''} \\ &+ \sum_{d_j} \mathrm{P}\int dE_1 \frac{V_{vd_j}(E,E_1)K_{d_jw}(E_1,E')}{E'-E_1}. \end{aligned} \tag{A24}$$

If we use Eqs. (A2) and (A3) and the fact that $K_{w'w} = 0$ and $K_{d_j w} = K_{w d_j} = 0$—proved previously in Eqs. (A23) and (A17)—the above equation for K_{vw} then becomes

$$K_{vw}(E,E') = V_{vw} \tag{A25}$$

for all v,w.

Lastly, we calculate elements of the block $\mathcal{K}_{\bar{v}\bar{v}}$. For any two vibrational channels v,v',

$$\begin{aligned} &K_{vv'}(E,E') \\ &= V_{vv'}(E,E') + \sum_{v''} \mathrm{P}\int dE'' \frac{V_{vv''}(E,E'')K_{v''v'}(E'',E')}{E'-E''} \\ &\quad + \sum_{w} \mathrm{P}\int dE'' \frac{V_{vw}(E',E'')K_{wv'}(E'',E')}{E'-E''} \\ &\quad + \sum_{d_j} \mathrm{P}\int dE_1 \frac{V_{vd_j}(E,E_1)K_{d_jv'}(E_1,E')}{E'-E_1}. \end{aligned} \tag{A26}$$

By Eqs. (A2) and (A3), $V_{vv'} = 0$ and $V_{vd_j}(E',E) = V_{vd_j}(E)$. Furthermore, by Eq. (A16), $K_{d_jv'}(E,E') = K_{v'd_j}(E',E) = V_{d_jv'}(E)$. Also, by Eq. (A25), $K_{wv'}(E'',E') = K_{v'w}(E',E'') = V_{wv'}$. Consequently, the above equation for $K_{vv'}$ becomes

$$\begin{aligned} K_{vv'}(E,E') &= \sum_{w} V_{vw}V_{wv'}\mathrm{P}\int \frac{dE''}{E'-E''} \\ &\quad + \sum_{d_j} \mathrm{P}\int dE_1 \frac{V_{vd_j}(E_1)V_{d_jv'}(E_1)}{E'-E_1}. \end{aligned} \tag{A27}$$

This further reduces to

$$K_{vv'}(E,E') = \sum_{d_j} \mathrm{P}\int dE_1 \frac{V_{vd_j}(E_1)V_{d_jv'}(E_1)}{E'-E_1} \tag{A28}$$

for all v,v' since the principal value of the integral on the right-hand side of Eq. (A27) is zero. The elements $K_{vv'}$ in Eq. (A28) can be calculated as in Eq. (21).

Finally, using Eqs. (A15), (A17), (A23), (A25), and (A28), the second-order reaction matrix can be written as in Eq. (23) of Sec. III B.

[1] M. Larsson and A. E. Orel, *Dissociative Recombination of Molecular Ions* (Cambridge University Press, Cambridge, UK, 2008).

[2] *Proceedings of the Eighth International Conference on Dissociative Recombination: Theory, Experiments and Applications (DR2010), 16–20 August 2010, Lake Tahoe, California, USA*, edited by A. E. Orel and S. L. Guberman (IOP, Bristol, 2011) [J. Phys.: Conf. Ser. **300** (2011)].

[3] *Proceedings of the Sixth International Conference on Dissociative Recombination: Theory, Experiments and Applications, 12–16 July 2004, Mosbach, Germany*, edited by A. Wolf, L. Lammich, and P. Schmelcher (IOP, Bristol, 2005) [J. Phys.: Conf. Ser. **4** (2005)].

[4] U. Fano, Phys. Rev. **124**, 1866 (1961).

[5] J. N. Bardsley, J. Phys. B **1**, 365 (1968).

[6] A. Giusti-Suzor, J. Phys. B **13**, 3867 (1980).

[7] M. J. Seaton, Rep. Prog. Phys. **46**, 167 (1983).

[8] C. H. Greene and Ch. Jungen, Adv. At. Mol. Phys. **21**, 51 (1985).

[9] *Molecular Applications of Quantum Defect Theory*, edited by Ch. Jungen (IOP, Bristol and Philadelphia, 1996).

[10] Ch. Jungen, in *Handbook of High Resolution Spectroscopy*, edited by M. Quack and F. Merkt (Wiley, Chichester/New York, 2011).

[11] A. Giusti-Suzor, J. N. Bardsley, and C. Derkits, Phys. Rev. A **28**, 682 (1983).

[12] T. Tanabe, I. Katayama, H. Kamegaya, K. Chida, Y. Arakaki, T. Watanabe, M. Yoshizawa, M. Saito, Y. Haruyama, K. Hosono, K. Hatanaka, T. Honma, K. Noda, S. Ohtani, and H. Takagi, Phys. Rev. Lett. **75**, 1066 (1995).

[13] C. Strömholm, I. F. Schneider, G. Sundström, L. Carata, H. Danared, S. Datz, O. Dulieu, A. Källberg, M. af Ugglas, X. Urbain, V. Zengin, A. Suzor-Weiner, and M. Larsson, Phys. Rev. A **52**, R4320 (1995).

[14] I. F. Schneider, C. Strömholm, L. Carata, X. Urbain, M. Larsson, and A. Suzor-Weiner, J. Phys. B **30**, 2667 (1997).

[15] H. Takagi, Phys. Scr. **T96**, 52 (2002).

[16] M. C. Stroe, A. I. Florescu, M. Fifirig, F. O. Waffeu Tamo, V. Ngassam, O. Motapon, and I. F. Schneider, Rom. Rep. Phys. **57**, 801 (2005).

[17] M. C. Stroe, M. Fifirig, F. O. Waffeu Tamo, O. Motapon, O. Crumeyrolle, G. Varin-Bréant, A. Bultel, P. Vervisch, A. Suzor-Weiner, and I. F. Schneider, in *Atomic and Plasma-Material Interaction Data for Fusion*, Vol. 14 (International Atomic Energy Agency, Vienna, 2008), p. 103.

[18] M. Stroe and M. Fifirig, Eur. Phys. J. D **61**, 63 (2010), and references therein.

[19] V. Sidis and H. Lefebvre-Brion, J. Phys. B **4**, 1040 (1971).

[20] Ch. Jungen and O. Atabek, J. Chem. Phys. **66**, 5584 (1977).

[21] V. Ngassam, A. Florescu, L. Pichl, I. F. Schneider, O. Motapon, and A. Suzor-Weiner, Eur. Phys. J. D **26**, 165 (2003).

[22] E. S. Chang and U. Fano, Phys. Rev. A **6**, 173 (1972).

[23] B. Vâlcu, I. F. Schneider, M. Raoult, C. Strömholm, M. Larsson, and A. Suzor-Weiner, Eur. Phys. J. D **1**, 71 (1998).

[24] A. Al-Khalili *et al.*, Phys. Rev. A **68**, 042702 (2003).

[25] O. Motapon, F. O. Waffeu Tamo, X. Urbain, and I. F. Schneider, Phys. Rev. A **77**, 052711 (2008).

[26] J. Tennyson, At. Data Nucl. Data Tables **64**, 253 (1996).

[27] V. Ngassam, O. Motapon, A. Florescu, L. Pichl, I. F. Schneider, and A. Suzor-Weiner, Phys. Rev. A **68**, 032704 (2003).

[28] M. Lange, J. Levin, G. Gwinner, U. Hechtfischer, L. Knoll, D. Schwalm, R. Wester, A. Wolf, X. Urbain, and D. Zajfman, Phys. Rev. Lett. **83**, 4979 (1999).

[29] L. H. Andersen, P. J. Johnson, D. Kella, H. B. Pedersen, and L. Vejby-Christensen, Phys. Rev. A **55**, 2799 (1997).

[30] M. O. Abdellahi, El Ghazaly, J. Jureta, X. Urbain, and P. Defrance, J. Phys. B **37**, 2467 (2004).